CORRECTION METHODS FOR EXCHANGE SOURCE TERMS IN UNSTRUCTURED EULER-LAGRANGE SOLVERS WITH POINT-SOURCE APPROXIMATION

T. Lesaffre*, A. Pestre*, E. Riber* and B. Cuenot*
lesaffre@cerfacs.fr
* CERFACS, 42 Avenue Gaspard Coriolis, 31100 TOULOUSE

Abstract
This paper provides a study of different methods to handle the limitations of the Lagrangian point-force approach in the context of unstructured LES solver. The point-force model, also called particle-in-cell model, relies on the assumptions that i) the diameter of the particle is small compared to the mesh cell size and ii) the spray is sufficiently homogeneous to ensure grid independence. Large deviations on the mass, momentum, and energy exchanges between the gas and liquid phases may occur if one of these assumptions is not verified. In particular, the more and more frequent use of refined grids for the carrier flow allowed by today's computer power leads to cell sizes of the order or smaller than the particle diameters.

Several methods are proposed in the literature to tackle this problem. However, they are usually suited for structured solvers where the neighboring cells are easily accessed. In the case of unstructured parallel 3D solvers handling several hundred thousand particles in unsteady flows, such methods are far too expensive. In the present work, two original methods adapted for spray calculations in unstructured solvers are implemented and compared: the particle-bursting method (PBM), and the multigrid method (MM). Two test cases are studied: the evaporation in a quiescent atmosphere and with convective effects.

The PBM is more accurate and improves greatly the accuracy of the results. However, this method is not grid-independent. The MM is independent of the Eulerian mesh refinement and provides satisfactory results depending on the Lagrangian mesh cell size.

Introduction
Spray combustion is encountered in aeronautical combustion chambers and many other industrial applications. Significant research efforts have been devoted to the understanding of these flows through theoretical [1], experimental [2], and numerical research [3-4]. To handle the large range of length and time scales introduced by a discrete liquid phase, different approaches have been developed which can be grouped in two categories, namely Eulerian or Lagrangian methods [5]. For applications with a large size-polydisperse spray, an efficient approach for modeling turbulent sprays is to use an Eulerian solver for the carrier flow coupled with a Lagrangian solver for the droplets, represented as point sources, i.e., without representing their interface. In this approximation, also called particle-in-cell or point-force approach, the coupling between the Eulerian carrier phase and the Lagrangian particles is limited to the exchange of mass, momentum, and energy in each cell volume, ignoring the droplet volume and the associated liquid volume fraction in the carrier phase.

This approximation has intrinsically two limitations. Firstly, the exchange source terms depend on the cell volume which means that the solution is not grid-independent. Secondly, the exchange source terms, i.e., drag, evaporation and heat transfer, are related to the gas conditions at infinity usually evaluated at the nodes of the cell containing the droplet, and therefore not correctly defined when the droplet size is close to the mesh cell size. Rangel [6] and more recently Sontheimer [7] estimated the relative error of the steady-state evaporation rate of a

single droplet in a quiescent environment to be higher than 50% when the ratio between the cell size (d_x) and the droplet diameter (d_p) is smaller than 2. These results were reproduced in this work to highlight the grid dependence of the total evaporation time of a droplet. Figure 1 shows that for a ratio d_x/d_p below 10, the error becomes non-negligible and is sufficient to impact the structure of a spray flame. In addition, the resulting fuel vapor field from an evaporating droplet is not well predicted when d_x/d_p becomes too small. Indeed, as shown in Direct Numerical Simulation (DNS) of evaporating droplets [8], the vapor forms around the droplet volume, i.e., in the neighboring cells when the droplet is larger than the cell, whereas the particle-in-cell approach always leads to a release of vapor inside the cell containing the droplet.

Different methods have been proposed in the literature to tackle these problems. Maxey and Patel [9] proposed a regularization of the source terms by a Gaussian kernel in the context of a viscous Stokes regime. The main parameter is the regularization length scale of the Gaussian kernel and different implementations have been derived for structured grids [10-11]. The implementation for unstructured grids is not straightforward as neighboring cells identification has a high CPU-cost. Capecelatro and Desjardins [12] proposed a filtered set of equations that implicitly regularize the source terms through diffusion, which they proved to be equivalent to the Gaussian kernel method. This work was later extended by Ireland and Desjardins [13] to correct the unperturbed quantities required for the models. Evrard [14] also proposed a method based on filtered equations. Poustis [15] applied a nonlinear diffusion equation to the source terms and obtained a grid-independent method. However, the explicit scheme used for time integration is not efficient enough to make the method affordable for realistic complex configurations and implicit time integration for non-linear equations is not straightforward. Zhang et al. [16] compared three different methods for the regularization of solid particles source terms: cube averaging method, diffusion-based method and two-grid method. The first two methods are again more suited to structured grids, although tedious work could extend them to unstructured grids. The two-grid method on the contrary appears to be more appropriate for unstructured grids.

In this paper, the two-grid method, called here multi-grid method (MM), is compared to another original point-source correction method based on a particle-bursting method (PBM) in the context of spray combustion.

The paper is structured as follows. Firstly, the governing equations are presented. Then, the coupling between these equations and the regularization methods are detailed. Finally, simulations of simple test cases are performed and results are analyzed.
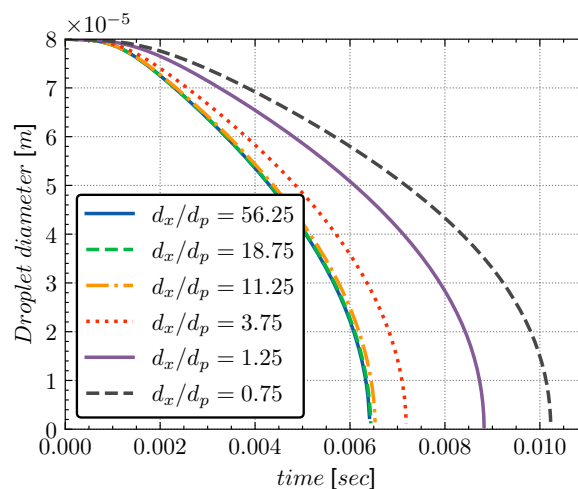
Figure 1. Time-evolution of the diameter of a kerosene droplet initially at 300 K in a quiescent atmosphere at temperature 2000 K and pressure 1 bar for various values of the ratio between the mesh cell size and the initial droplet diameter.

2 Governing equations

This section provides details on the coupling between the gas flow transport equations and the Lagrangian equations for particles. For the sake of simplicity and easier evaluation of the methods, only mass and heat exchange source terms are considered here, meaning that no drag force is applied. As a consequence, only species and energy equations are presented here. The whole set of equations can be found in [4].

2.1 Gas phase equations

The conservation equations for species write:

$$\frac{\partial \rho Y_k}{\partial t} + \frac{\partial \rho (u_j + V_{j,k}) Y_k}{\partial x_j} = \dot{\omega}_k + S_k^{l \to g} \quad \text{for } k = 1, N_{spec} \tag{1}$$

where ρ is the gaseous mass density, u is the velocity, and Y_k is the mass fraction of species k. $\dot{\omega}_k$ is the chemical source term of species k and is equal to zero for non-reactive cases while $S_k^{l \to g}$ corresponds to the mass transfer from the liquid phase to the gaseous phase. The diffusion velocity $V_{j,k}$ is modeled with Hirschfelder and Curtiss approximation [17], and constant species Schmidt numbers Sc_k, and Prandtl number Pr are used.

The energy equation for the gas phase writes:

$$\frac{\partial \rho E}{\partial t} + \frac{\partial \rho E u_j}{\partial x_j} = -\frac{\partial q_j}{\partial x_j} - \frac{\partial u_i P \delta_{ij}}{\partial x_j} + \frac{\partial u_i \tau_{ij}}{\partial x_j} + \dot{Q} + \dot{\omega}_T + S_E^{l \to g} \tag{2}$$

where E is the total energy, q_j is the heat diffusive flux, P is the pressure, τ_{ij} is the stress tensor. $\dot{Q}$ is the heat source term and is equal to zero in adiabatic calculations, and $\dot{\omega}_T$ is the heat release due to combustion and is also null for non-reactive cases. $S_E^{l \to g}$ is the energy transfer from the liquid phase to the gaseous phase.

2.2 Liquid phase equations

The particle motion is described with a Lagrangian approach based on the Basset-Boussinesq-Oseen equations [18]. The evaporation model follows Abramzon-Sirignano [19] with the Ranz-Marshall correlations [20] for Sherwood and Nusselt numbers. Then, the time evolution of the particle mass m_p obeys:

$$\frac{dm_p}{dt} = \dot{m}_p^n = -\pi \, d_p \, \text{Sh} \, \rho_f D_F \, ln(1 + B_M) \tag{3}$$

where d_p is the particle diameter, and Sh is the Sherwood number and D_F is the fuel species diffusivity. The density ρ_f is estimated in the liquid film around the droplet through the classical 1/3 rule [21]. Finally, the mass Spalding number B_M is computed as:

$$B_M = \frac{Y_{F,s} - Y_{F,\infty}}{1 - Y_{F,s}} \tag{4}$$

where $Y_{F,s}$ is the fuel mass fraction at the interface, determined by the use of Clausius-Clapeyron and $Y_{F,\infty}$ is the fuel gaseous mass fraction in the environing gas. Typically, in a particle-in-cell approach, $Y_{F,\infty}$ is computed as the interpolated fuel gaseous mass fraction at the droplet location.

The droplet temperature evolution is driven by the Nusselt number and the temperature Spalding number B_T, computed following [19].

3. Coupling between gas and liquid phase

In a particle-in-cell approach, the two-way coupling between the liquid and gaseous phases is implemented with a first-order interpolation between the droplet positions and the grid nodes. Then, the mass transfer from the liquid phase to the gaseous phase in Eq. (1) is expressed as:

$$S_F^{l \to g} = \frac{1}{\Delta V} \sum_{n=1}^{N_p} \Psi(x_p^n) \dot{m}_p^n \qquad (5)$$

where ΔV is the volume associated with the node, N_p the number of particles, and $\Psi(x_p^n)$ is a first-order interpolator between the particle position and the grid nodes.

The energy transfer from the liquid phase to the gaseous phase in Eq. (2), neglecting drag, writes as:

$$S_E^{l \to g} = \frac{1}{\Delta V} \sum_{n=1}^{N_p} \Psi(x_p^n) \phi_g \qquad (6)$$

where ϕ_g is the total heat flux due to evaporation including conductive heat flux and the latent heat of evaporation.

Eqs. (5) and (6) express that the source terms associated to a particle are only distributed to the nodes of the cell containing the particle. A direct consequence is that the intensity of the source terms increases when the mesh is refined: in Eq. (5), the source terms $\dot{m}_p^n$ do not change while the node volume decreases. Besides not being grid-independent, this implementation may lead to numerical stiffness when the source terms become too large. This also produces an artificial local increase in the fuel vapor and decrease in temperature which can then slow down the evaporation process.

In order to resolve the above issues, two methods are proposed and evaluated herein. They are described in the following.

3.1 Particle-Bursting method

The particle-bursting method (PBM) performs a spatial regularization by acting on the particles rather than on the source terms as usually done in the literature [15]. The idea is to create artificial particles that will spread the source terms of a particle outside the containing cell, while guaranteeing conservation of all quantities. This is achieved thanks to the concept of particle parcels [22], in which each numerical particle represents *rparcel* physical particles, ideally having exactly the same properties (position, mass, velocity, energy). Usually particle parcels are used to decrease the number of particles to compute, allowing to reduce the CPU cost of simulations with a high number of particles [5]. In such case, the *rparcel* number is above one. However, the *rparcel* number can also be lower than one, for example in order to reach faster statistical convergence. In the PBM method, a *rparcel* number lower than one is used to distribute the source term of a given particle to the neighboring cells while conserving mass, momentum, and energy. This is illustrated in Fig. 2, where N_{burst} particles are created to represent the source term of an initially single particle, leading to a *rparcel* equal to $1/N_{burst}$. Note that Lagrangian particle tracking is mesh-free so that the penalty induced by unstructured meshes disappears with the PBM.

To make the PBM independent of the mesh, the control volume containing the burst particles may be fixed to a constant value. In the literature, the characteristic regularization length $\mathcal{L}$ is usually expressed as a multiple of the particle diameter, e. g. $\mathcal{L} = 6\,d_p$ [15]. A similar approach is followed here. A cubic control volume taken as $(Bd_p)^3$ is adopted, B being a proportionality coefficient depending on the d_x/d_p ratio. The burst particles are then

randomly distributed inside this control volume. The number of particles to be burst can be estimated by:

$$N_{burst} = A_b \frac{V_{control}}{V_p} = A_b \frac{(\text{Bd}_p)^3}{\frac{\pi}{6} d_p^3} = \frac{6}{\pi} A_b B^3 \tag{7}$$

where the particle volume V_p is the same for all burst particles, and the constant A_b gives the ratio of the total volume of all burst particles over the control volume. A_b is to ensure a smooth distribution of source terms inside the control volume and should be chosen carefully.
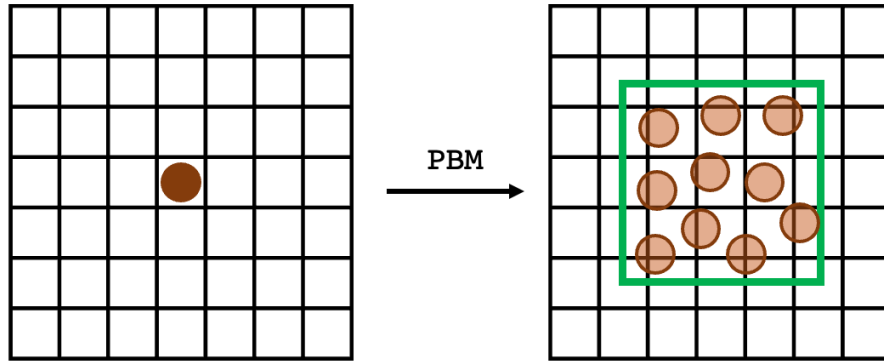
Figure 2. Principle of the particle-bursting method. Left: initial particle. Right: distributed burst particles in the control volume delimited by the green lines.

3.2 Multigrid method

The multigrid method (MM) consists in decoupling the domain discretization for the gas and the liquid phases. Indeed, Lagrangian particle tracking is a mesh-free approach, and a grid is required only for the phase exchange source terms. While the Eulerian gas calculation calls for a mesh as much refined as possible to reduce the impact of the subgrid models, the optimum mesh for the exchange source terms depends on the particle size. Therefore, a practical solution is to use two distinct meshes for the gas phase and the exchange source terms, associated with interpolation operators. For an efficient implementation on parallel computers, the Eulerian and the Lagrangian solvers are run independently on distinct processors, relying on an external coupler library such as cwipi [23] to exchange the fields of interest. This communication scheme is summarized in Fig. 3. The same library is used to apply the interpolation operators, which is not straightforward with unstructured meshes.
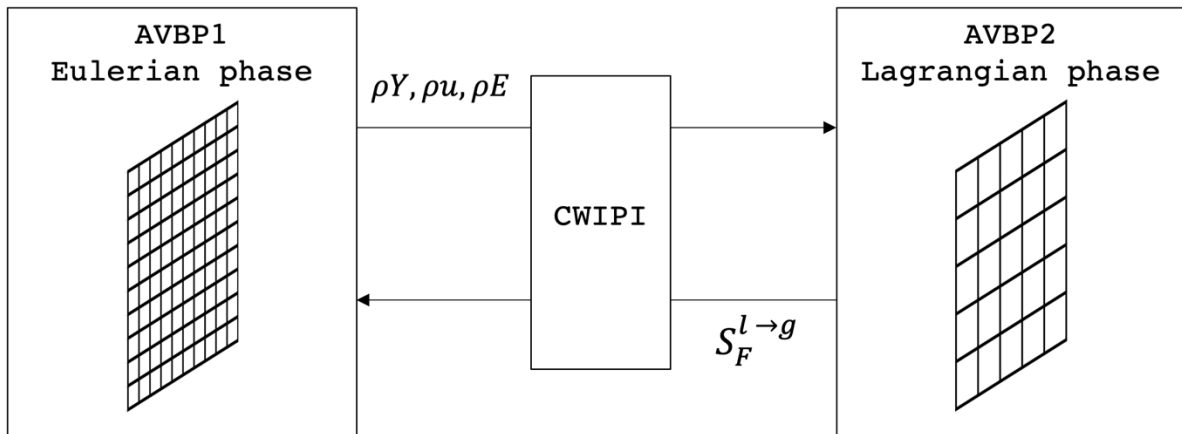
Figure 3. Communication scheme used for the multi-grid method (MM) implementation

The great advantage of MM is to allow the choice of the control volume for the exchange source terms independently of the Eulerian grid. In that sense, it makes the two-phase simulation grid-independent regarding the Eulerian mesh. Similarly to the PBM, the control volume for the exchange source terms should be chosen with care and can be formulated as $(Bd_p)^3$, representing now the cell size of the Lagrangian solver mesh.

4. Numerical Simulations

In order to evaluate both methods in terms of accuracy and grid sensitivity, two simple test cases are first studied, corresponding to the evaporation of a single droplet (i) in a quiescent atmosphere (case A) and (ii) with a non-zero velocity (case B). In the second case, particle drag is ignored in order to keep a constant relative velocity and ease the analysis.

The evaporation of a droplet in a quiescent atmosphere is a canonical case which has been vastly studied [1]. Here we consider a 80 μm diameter droplet of kerosene located at the center of a hot air volume of 91 mm^3 at 2000 K and 1 bar. The two regularization methods are tested on various meshes, summarized in Table 1.

Table 1. Meshes for case A.

Number of cells	1	27	125	3375	91125	421875
d_x/d_p	56.25	18.75	11.25	3.75	1.25	0.75

In the second test case the same droplet moves at a constant speed of 10 m/s within the same hot air flow at 1 m/s, keeping the relative velocity constant at $u^* = u_p/u_g = 10$. The domain considered is a rectangular box with a square base (4.5 mm x 4.5 mm) and a length of 67.5 mm. Different meshes are also considered and summarized in Table 2.

Table 2. Meshes for case B.

Number of cells	405	1875	16875	1366875
d_x/d_p	18.75	11.25	3.75	1.25

Both cases are run with the AVBP solver (*https://www.cerfacs.fr/avbp7x/*) with a central finite difference Lax-Wendroff scheme [24], being second order in time and space. The Navier-Stokes equations are solved in their non-reactive form and include three species: a liquid species $C_{10}H_{20}$, taken as a kerosene surrogate, and the air species O_2 and N_2.

5. Results and discussion

The PBM and MM differ by the number of user-defined parameters. While in the MM, only the mesh cell size in the Lagrangian solver needs to be fixed, the PBM requires in addition to decide the number of burst particles N_{burst}. This section is therefore divided into two parts. Firstly, the influence of N_{burst} in PBM is studied. Then, a comparative study of both methods (PBM and MM) in terms of grid dependence is presented. Effects of the regularization length-scale and convective effects are particularly highlighted.

5.1 PBM: Effect of N_{burst}

The concept of the PBM is to spread the source terms in the control volume by distributing them over a number of burst particles N_{burst}, or equivalently a volume ratio A_b. If this parameter should not impact the mesh dependence (controlled by the size of the control volume), it has a great impact on the numerical stability. Figure 4 compares the spatial profiles

of the mass source term obtained with various values of A_b in case A after 0.5 ms for a control volume corresponding to B = 11 (left) and B = 6 (right). In both cases, the value of $A_b = 0.1$ appears to be a good compromise. Lower values induce ripples in the source term whereas a higher value does not affect the source term anymore, indicating that convergence has been reached. $A_b = 0.1$ will then be used for the rest of the study.

An interesting feature can be observed in Fig. 4 showing at the considered time a slightly lower mass source term at the center, i.e., at the location of the droplet point source. This is due to the surrounding gas conditions seen by the particles, which differ between the cell containing the initial droplet and the neighboring cells. As illustrated in Fig. 5, the gas temperature is lower and the fuel vapor mass fraction is higher at the center at the considered time. This is due to thermo-diffusive effects which smoothen the fields inside the total gaseous volume. This is confirmed by the time evolution of the mass source term plotted in Fig. 6. At the first iteration, the mass source term is uniform in the control volume as the conditions seen by the burst particles are the same. Then, due to diffusion effects, the source term decreases at the center of the control volume which means that the burst particles at the border of the control volume evaporate quicker than at the center. Towards the end of the droplet lifetime, the mass source term is higher at the center as the burst droplets at the border of the control volume are already evaporated.
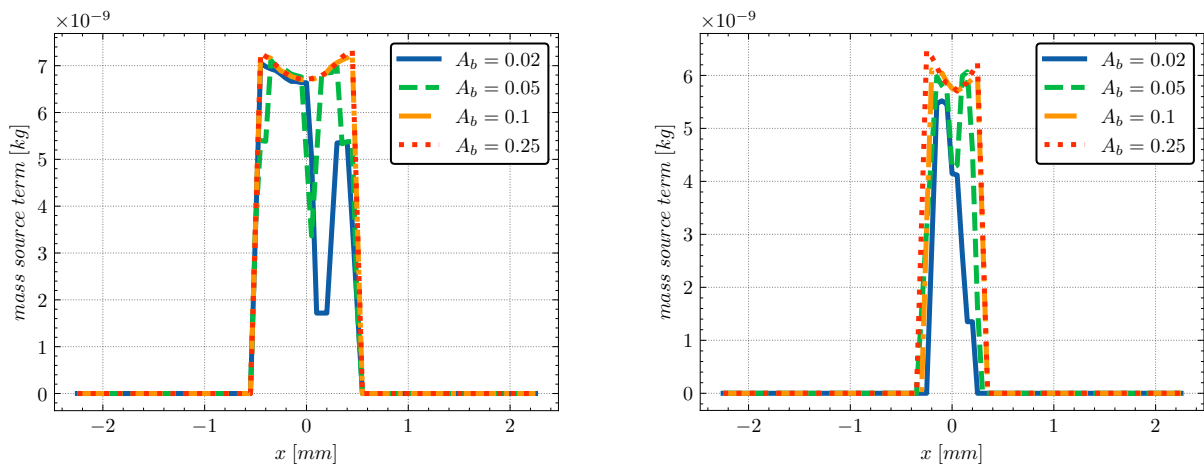
Figure 4. Mass source term in case A and $d_x/d_p = 1.25$ for the control volume with B=11.25 (left) and $B = 6$ (right) at t=0.5 ms using the PBM.
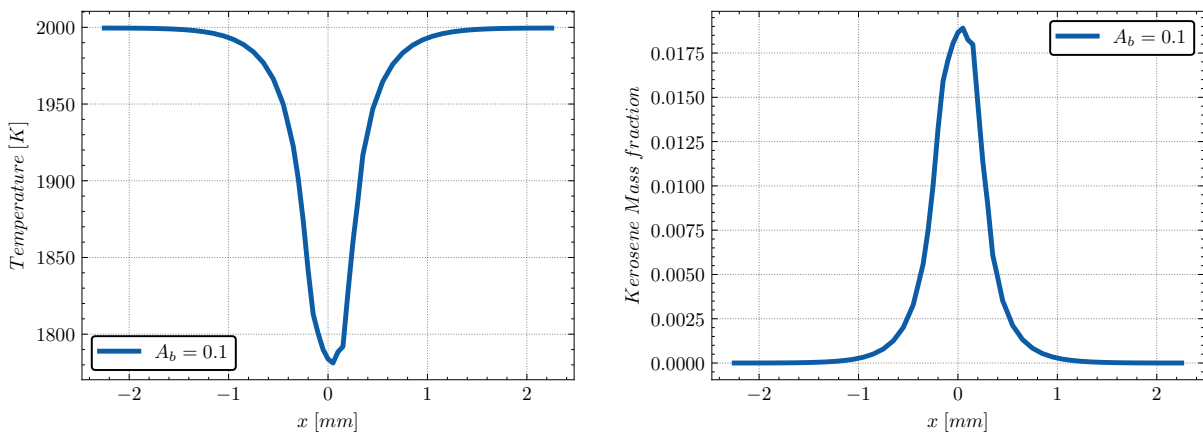
Figure 5. Temperature and fuel gaseous mass fraction in case A and $d_x/d_p = 1.25$ for the control volume with B=11.25 at t=0.5 ms using the PBM.
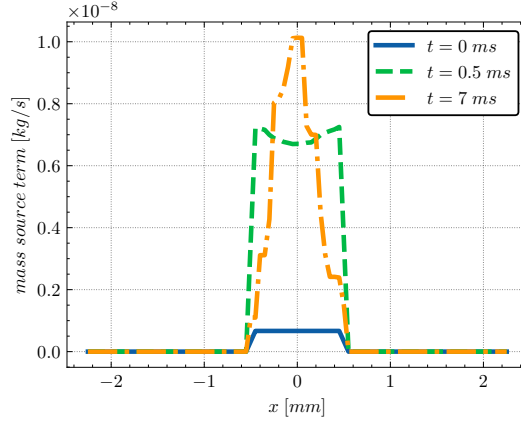
Figure 6. Mass source term in case A and $d_x/d_p = 1.25$ for control volume B=11.25 for different instants using the PBM.

5.2 Grid independence

By introducing a control volume, both PBM and MM reduce the grid dependence of two-phase simulations with Lagrangian particle tracking. In the PBM, this volume is prescribed by the parameter B while, in the MM, it is directly the cell size of the mesh used in the Lagrangian solver to compute the exchange source terms. The question then arises of what should be the size of this control volume. As the fuel vapor is released at the surface of the droplet, a realistic control volume should be close to the size of the evaporated droplet, which means very fine meshes. However, it would have a detrimental effect on the evaporation model prediction which requires unperturbed flow quantities and would provide numerically stiff problems. Therefore, larger control volumes are used, introducing some errors that are evaluated in this section.

The evaporation in a quiescent environment (case A) is most sensitive to mesh size / control volume, as transport phenomena are limited to thermal and molecular diffusion. Starting from the case with the highest ratio $d_x/d_p = 56.25$ without using a control volume, the relative deviation induced by mesh refinement can be computed for all other cases, with and without source term regularization by both PBM and MM. The objective is twofold: evaluating the impact of these methods on grid dependence and on numerical stiffness.

The droplet lifetimes obtained with the PBM and with the MM for two values of B and as functions of the Eulerian grid resolution are shown in Fig. 7. It can be observed that both methods reduce the relative deviation for the fine meshes, i.e, they reduce mesh dependence.
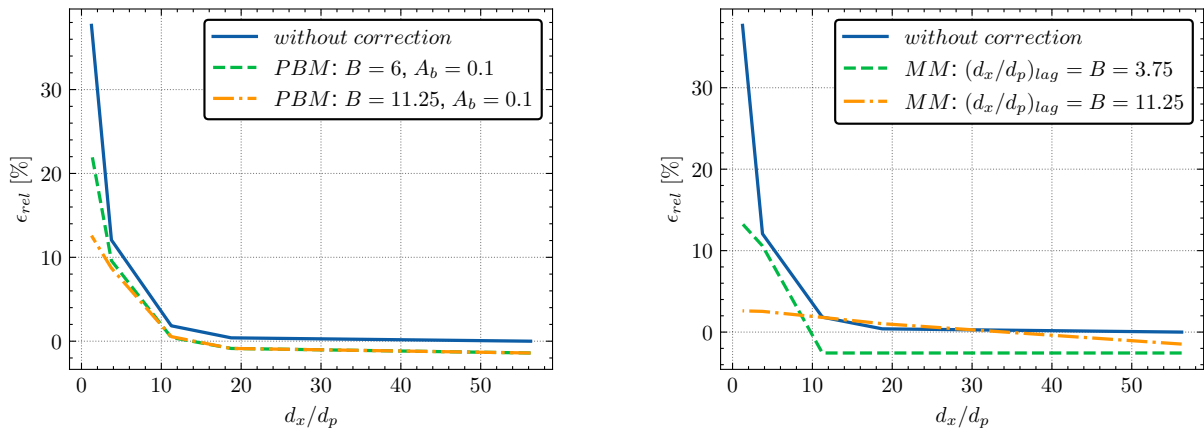
Figure 7. Relative deviation on the droplet lifetime in case A depending on the parameter B for the PBM (left) and the MM (right).

In the case without correction, i.e., use of a control volume, and consistently with results of Fig. 1, the relative deviation remains close to 0 down to d_x/d_p =11.25. Indeed, for these high

volume ratios the impact of the source terms on the gas stays small and does not significantly change the gas fuel mass fraction and temperature used in Eq. (3). On the contrary the deviation increases rapidly when the volume ratio decreases, reaching about 38% for the finest Eulerian grid. This deviation is well reduced with the PBM, and even more with the MM.

By construction, the PBM improves the results only when the control volume exceeds the cell size, and the improvement increases with B: using $B = 6$ reduces the deviation from 38% to 22%, while $B = 11.25$ divides the deviation by 3. Similarly, the MM is effective with values of B higher than the size ratio d_x/d_p : using $B = 11.25$ has a strong impact on the case with a size ratio of 3.75 and 1.25 but has little or no impact for higher d_x/d_p. Note that by construction MM gives the same deviation than the case without correction when $B = d_x/d_p$. Overall, the MM appears more efficient than the PBM: using $B = 11.25$ with the MM reduces the deviation to 3% for d_x/d_p=1.25 while it stays at 12% for the PBM.

It is interesting to compare the impact of the PBM and the MM on spatial profiles. Figure 8 reports the mass source term for both methods, in the case with B=11.25. The width of the maximum of the source term is the same for both methods as the regularization length-scale is the same. However, the shape at the border is different and directly linked to the Eqs. (5) and (6) formulations. In the PBM, the first-order interpolation operator, $\Psi(x_p^n)$, is directly applied on the fine Eulerian mesh, which means that the source term of each droplet is relaxed towards a null value on a length equal to $d_x = 1.25 d_p$. On the other hand, for the MM, $\Psi(x_p^n)$ is first applied on the coarse mesh used for the Lagrangian source terms and then interpolated on the fine Eulerian mesh. Therefore, the relaxation of the source term towards zero extends over a greater length of $11.25 d_p$. This larger relaxation leads to more diffuse fields of temperature and fuel mass (Fig. 9) for the MM which explains why it provides better results under mesh refinement.
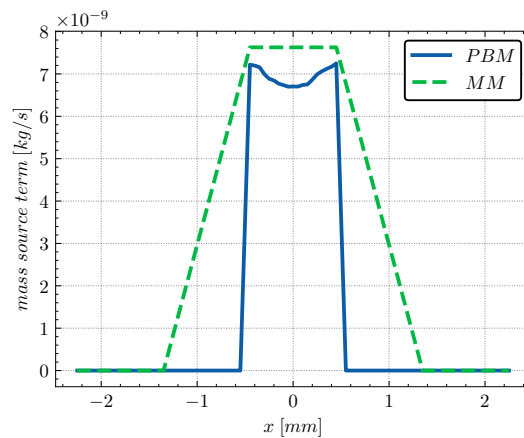
Figure 8. Spatial profiles of mass source terms for PBM and MM with B=11.25 and $d_x/d_p = 1.25$ at 0.5 ms.

The case B with convective effects (without drag), more representative of practical situations, is now studied following the same methodology as for case A. The results for PBM and MM are compared in Fig. 10, left and right respectively. Deviations are overall smaller than in case A, even for the uncorrected case. This is expected as the local cell variations of fuel mass fraction and gas temperature have less impact on the particle which moves away to another cell. The PBM helps decreasing the deviation on the droplet lifetime for the finest mesh but does not improve the results for $d_x/d_p = 3.75$ as it was the observed in case A.

This can be explained by an asymmetry of the evaporation of bursting particles, which do not see the same gas state depending if they are located ahead or in the wake of the initial

droplet, where evaporation already occurred. Figure 11 illustrates this effect, showing a faster evaporation at the front where the mass source term is higher and where the temperature is close to 2000 K while it is below 1800 K at the back of the control volume. Hence, the liquid volume fraction becomes higher at the back of the volume. This asymmetry is much sensitive to the Eulerian mesh and limits the regularization effect of the PBM.
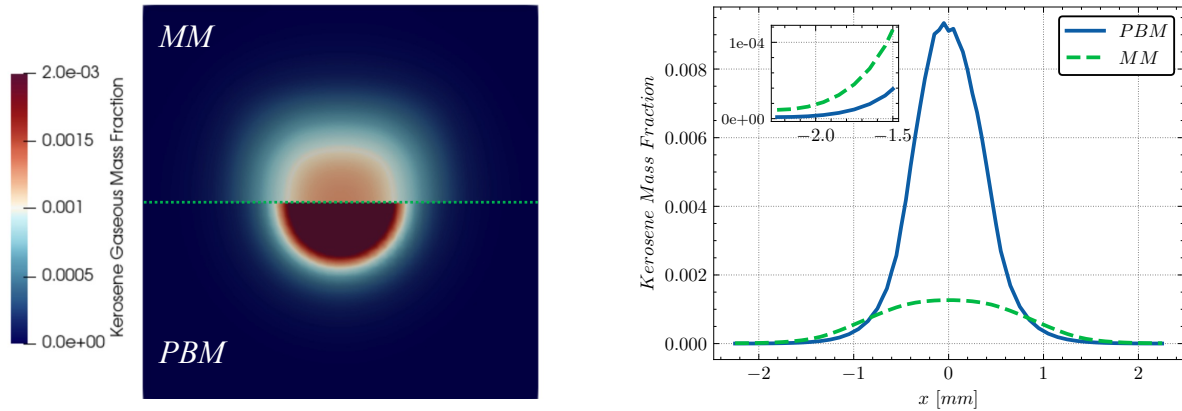
Figure 9. Kerosene mass fraction cut-plane field (left) and profile along a line (right) for PBM and MM with B=11.25 and $d_x/d_p = 1.25$ at 0.5 ms.

On the other hand, the MM shows an extremely good behavior and reaches well grid independence in the case with B=11.25 (Fig. 10 right), with a relative deviation less than 2% whatever the Eulerian mesh is used. Even the smaller B gives a deviation below 5%, to be compared to the almost 15% in case A.
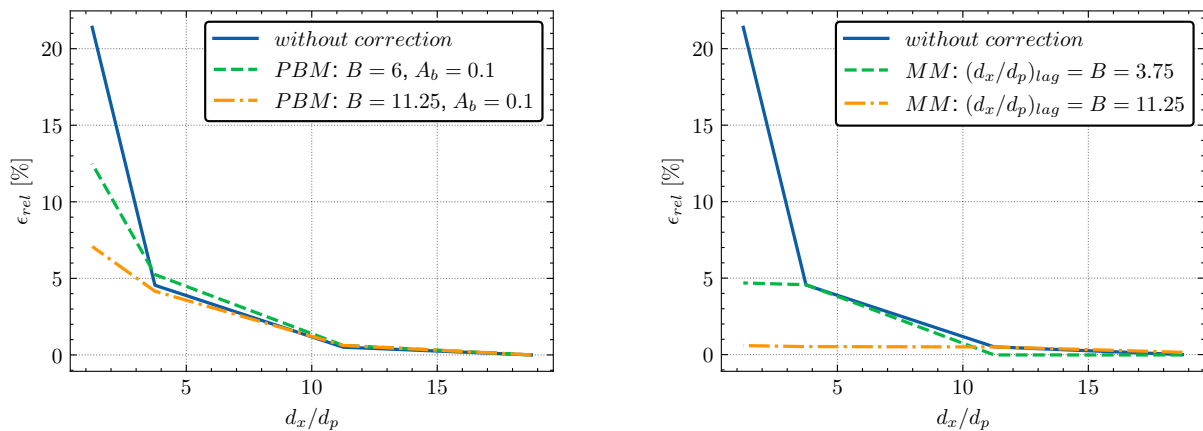
Figure 10. Relative deviation on the droplet lifetime in case B depending on the parameter B for the PBM (left) and the MM (right).

Conclusion

In this study, two original methods have been proposed to correct exchange source terms between phases when the Eulerian grid for the carrier phase becomes too fine and close to the diameter of the droplets. The first presented method based on particle bursting proved to be efficient in reducing the impact of mesh refinement on the solution. However, grid independence was not reached due to remaining mesh-sensitive inhomogeneity of the gas state around the droplets. The second method that was developed is a multi-grid approach. This method allowed to make the solution independent of the Eulerian cell size for sufficiently coarse secondary mesh. It was also found that convective effects help grid independence with the MM.

These results are preliminary and other two-phase flow conditions should be tested, in particular with higher particle load and with chemistry effects considered to assess the robustness of each method. Moreover, the computational cost of both methods should be investigated. In particular the multi-grid method will be sensitive to particle load balancing and will require an optimized distribution of the computational resources between the two solvers. This will be the subject of future work.
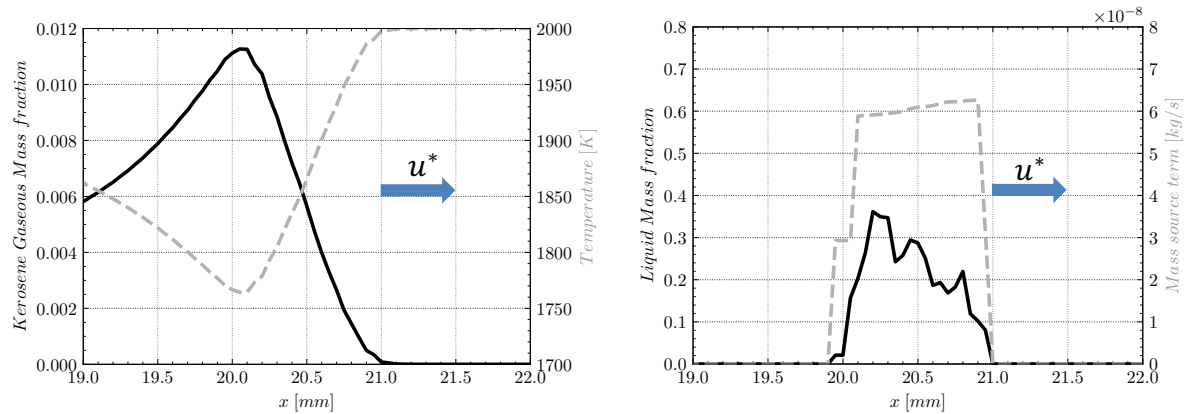
Figure 11. Kerosene Mass fraction and Temperature (left), Liquid Mass fraction and Mass source term (right) along the flow direction in case B after 2 ms for the PBM with B=11.25 and d_x/d_p= 1.25.

Nomenclature

A_b	Coefficient in the PBM method to control the volume occupied by the burst particles in the volume of control
A_p	Coefficient in the TLM method to limit density variation
B	Edge length of the volume of control in the PBM
B_M	Spalding Mass Number
d_p	Droplet diameter
d_x	Characteristic length of a mesh cell
MM	Multi-grid Method
N_{burst}	Number of burst particles in the PBM
PBM	Particle-Bursting Method
rparcel	Number of physical particles represented by one numerical particle
$\Psi(x_p^n)$	First order interpolation operator

References

[1] Sirignano, W. A., *Fluid Dynamics and Transport of Droplets and Sprays. Second Edition*. Cambridge University Press, New York, 2010.

[2] Agarwal, A. K., Park, S., Dhar, A., Lee, C. S., Park, S., Gupta, T., Gupta, N. K., "Review of experimental and computational studies on spray, combustion, performance, and emission characteristics of biodiesel fueled engines". *Journal of Energy Resources Technology, Transactions of the ASME, 140* (2018).

[3] Felden, A., Esclapez, L., Riber, E., Cuenot, B., Wang, H., "Including real fuel chemistry in LES of turbulent spray combustion". *Combustion and Flame, 193*, 397–416 (2018).

[4] Paulhiac, D., Cuenot, B., Riber, E., Esclapez, L., Richard, S., "Analysis of the spray flame structure in a lab-scale burner using Large Eddy Simulation and Discrete Particle Simulation". *Combustion and Flame, 212*, 25–38 (2020).

[5] Riber, E., Moureau, V., García, M., Poinsot, T., Simonin, O., "Evaluation of numerical strategies for large eddy simulation of particulate two-phase recirculating flows". *Journal of Computational Physics, 228(2), 539–564* (2009).

[6] Rangel, R. H., Sirignano, W. A., "An evaluation of the point-source approximation in spray calculations". *Numerical Heat Transfer; Part A: Applications*, *16*(1), 37–57 (1989).

[7] Sontheimer, M., Kronenburg, A., Stein, O. T, "Grid dependence of evaporation rates in Euler–Lagrange simulations of dilute sprays". *Combustion and Flame*, *232* (2021).

[8] Schlottke, J., Weigand, B. "Direct numerical simulation of evaporating droplets*". Journal of Computational Physics 227*, 5215–5237 (2008).

[9] Maxey, M. R., Patel, B. K., "Localized force representations for particles sedimenting in Stokes*". International Journal of Multiphase Flow 27, 1603-1626* (2001).

[10] Ling, Y., Zaleski, S., Scardovelli, R., "Multiscale simulation of atomization with small droplets represented by a Lagrangian point-particle model". *International Journal of Multiphase Flow 76, 122-143* (2015).

[11] Khare, P., Wang, S., Yang, V, "Modeling of finite-size droplets and particles in multiphase flows". *Chinese Journal of Aeronautics* (2015).

[12] Capecelatro, J., Desjardins, O, "An Euler – Lagrange strategy for simulating particle-laden flows". *Journal of Computational Physics*, *238*, 1–31 (2013).

[13] Ireland, P. J., Desjardins, O, "Improving particle drag predictions in Euler-Lagrange simulations with two-way coupling". *Journal of Computational Physics* (2017).

[14] Evrard, F., Denner, F., van Wachem, B, "A multi-scale approach to simulate atomisation processes". *International Journal of Multiphase Flow*, *119*, 194–216 (2019).

[15] Poustis, J. F., Senoner, J. M., Zuzio, D., Villedieu, P, "Regularization of the Lagrangian point force approximation for deterministic discrete particle simulations". *International Journal of Multiphase Flow*, *117*, 138–152 (2019).

[16] Zhang, J., Li, T., Ström, H., & Løvås, T, "Grid-independent Eulerian-Lagrangian approaches for simulations of solid fuel particle combustion". *Chemical Engineering Journal*, *387* (2020).

[17] Hirschfelder, J.O., Curtiss, C.F., Bird, R.B., *Molecular Theory of gases and liquids*. John Wiley & Sons, New York, 1969.

[18] Maxey, M., Riley, J., "Equation of motion for a small rigid sphere in a nonuniform flow", *Phys. Fluids, 26 (4), 883–889* (1983).

[19] Abramzon, B., Sirignano, W. A., "Droplet vaporisation model for spray combustion calculations", *Int. J. Heat Mass Transf., 9,* 1605–1618 (1989).

[20] Ranz, W., Marshall, W., "Evaporation from drops", *Chem. Eng. Prog., 48 (3), 141–146* (1952).

[21] Hubbard, G., Denny, V., Mills, A., "Droplet evaporation: effects of transients and variable properties", *Int. J. Heat Mass Transf., 18 (9), 1003–1008* (1975).

[22] Dukowicz, J., "A particle-fluid numerical model for liquid sprays". *Journal of Computational Physics, 35, 229-253* (1980).

[23] Refloch, A., Courbet, B., Murrone, A., Villedieu, P., Laurent, C., Gilbank, P., Troyes, J., Tessé, L., Chaineray, G., Dargaud, J.B., Quémerais, E., Vuillot, F., "Cedre Software". *Aerospace Lab Journal* (2011).

[24] Lax, P., Wendroff, B., "Systems of conservation laws", *Communications on Pure and Applied Mathematics, 13: 217-237* (1960).